High-order spectral volume scheme for multi-component flows using non-oscillatory kinetic flux☆

Na Liu[a,b,c], Xihua Xu[a], Yibing Chen[a,c,*]

[a] *Institute of Applied Physics and Computational Mathematics, Beijing 100088, P.R. China*
[b] *Software Center for High Performance Numerical Simulation, Beijing 100088, P.R. China*
[c] *Laboratory of Computational Physics, Beijing 100088, P.R. China*

Abstract

In this paper, an arbitrary high-order compact method is developed for compressible multi-component flows with a stiffened gas equations of state(EOS). The main contribution is combining the high-order, conservative, compact spectral volume scheme(SV) with the non-oscillatory kinetic scheme(NOK) to solve the quasi-conservative extended Euler equations of compressible multi-component flows. The new scheme consists of two parts: the conservative part and the non-conservative part. The original high order compact SV scheme is used to discretize the conservative part directly. In order to treat the equation of state of the stiffened gas, the NOK scheme is utilized to compute the numerical flux. Then, careful analysis is made to satisfy the necessary condition to avoid unphysical oscillation near the material interfaces. After that, a high-order compact scheme for the non-conservative part is obtained. This new scheme has the following advantages for numerical simulations of compressible multi-component stiffened gas: high order accuracy with compact stencil and oscillation-free near the material interfaces. Numerical tests demonstrate the good performance and the efficiency of the new scheme for multi-component flow simulations.

Keywords: multi-component flows; spectral volume method; NOK flux;

☆Supported by National Natural Science Foundation of China(Grant No.11101047, 11501043, 91430218), and the National High Technology Research and Development Program of China(Grant No. 2015AA01A304).

*Corresponding author
Email address: chen_yibing@iapcm.ac.cn (Yibing Chen)

stiffened gas; compact stencil

1. Introduction

In recent years, the numerical simulation of compressible multi-component flows has attracted much attentions in a wide range of field, such as ICF, energy, water conservancy and so on. When a compressible inviscid flow includes several components, the flow can be modeled by the so-call extended Euler equations[1]. It includes the traditional compressible Euler equations

$$\begin{pmatrix} \rho \\ \rho U \\ \rho E \end{pmatrix}_t + \begin{pmatrix} \rho U \\ \rho U^2 + P \\ (\rho E + P)U \end{pmatrix}_x = 0, \tag{1}$$

and the species equation

$$\phi_t + U\phi_x = 0, \tag{2}$$

which expresses the dynamics of the fluid composition. ϕ has many choices, such as the specific heat ratio γ, the mass fraction $Y = \frac{\rho_1}{\rho_1+\rho_2}$, the level-set function and so on. Here ρ, U, P, E denote density, velocity, pressure and the total energy, respectively, and ρ_1, ρ_2 represent density of two different components.

The stiffened gas is considered in this paper, and its EOS is

$$P = (\gamma - 1)\rho e - \gamma p_\infty, \tag{3}$$

where the inner energy $e = E - \frac{1}{2}U^2$.

In the early work, the traditional conservative schemes are used for the multi-component flow simulations. However, spurious oscillations will be produced near the material interfaces. Great efforts had been made to conquer this problem [1, 2, 3, 4]. In [2], Abgrall analyzed the cause of these oscillations and proposed a quasi-conservative method using the approximate Riemann solver of Roe. Subsequently, this method was extended to more general equations of state [5] successfully.

Besides the Godunov-type method, the gas kinetic scheme(GKS) [6, 7, 8] provides an alternative for solution evolution. The solution of the particle distribution function on the cell interface is obtained by solving the Bhatnagar-Gross-Krook(BGK) model of Boltzmann or collisionless Boltzmann equation, and then all the macroscopic variables can be regained subsequently. Comparing to the Godunov-type method, GKS provides more physical information of the flow and is free from constructing Riemann-solver. It turns out that GKS provides robust and accurate numerical solutions for various unsteady compressible flows, see [6, 9, 10, 11] and references therein.

In the past decades, the GKS has been successfully applied to multi-component flows. In the previous work, see[12, 13, 14, 15, 16], the full conservative schemes are often used. They can work well in case of small difference between two species. However, oscillations of pressure and velocity are always observed near the contact discontinuities and material interfaces. In [17], Chen and Jiang analyzed the cause of oscillations and found a remedy, a quasi-conservative scheme, for the ideal gas. Later, they extended the scheme to solve more general material and named it as NOK scheme[18].

Most of the schemes for multi-component flows mentioned above are at most second order accuracy. Some higher order schemes have been utilized to multi-component flow simulation recently. Johnsen [19] successfully extended WENO scheme to solve the extended Euler equations by implementing the quasi-conservative method and HLLC Riemann solver. The scheme greatly improved the resolution of the interfaces and shock waves. However, it is not a compact scheme. Different from Johnsen's way, Qiu et al. [20] used DG method to achieve high order accuracy. Compared to WENO, the DG method is a compact scheme which assumes a high order data distribution in each cell. However, high order surface and volume integrals are necessary, which may be expensive to compute. Recently, another high-order scheme with compact stencil called the spectral volume method(SV)[21, 22, 23] was developed by Wang. Similar to the DG method, only inner information is needed to reconstruct a high order approximation in the spectral volume. So SV method shares many advantages

with DG method, such that they are all compact and easy to parallel. In [21], Wang pointed out that SV method did not need volume integral and had a less restrictive stability limit, which made it more efficient than DG method.

The main objective of this paper is to design a spectral volume method using non-oscillatory kinetic flux, named as SVNOK scheme, for multi-component flow simulation which is high-order accurate and stencil-compact, at the same time can suppress unphysical oscillations near shock waves and material interfaces. This article is organized as follows. The implementation of the new scheme is presented in Section 2, including the spatial and time discretization. Section 3 shows the numerical tests that illustrate the good performance of the scheme. The last section is the conclusion.

2. The numerical scheme

In 1D case, suppose the domain Ω is discretized into N nonoverlapping cells $\{S_i = [x_{i-1/2}, x_{i+1/2}] \subset \Omega, i \in \mathbb{Z}\}$. Each of them is called a spectral volume. To design a $\mathbf{k}$-th order accurate scheme, each spectral volume S_i is subdivided into $\mathbf{k}$ control volumes(CVs), denoted by

$$C_{i,j} = (x_{i,j-1/2}, x_{i,j+1/2}), j = 1, \ldots, \mathbf{k},$$

where $x_{i,1/2} = x_{i-1/2}$ and $x_{i,\mathbf{k}+1/2} = x_{i+1/2}$. Let $h_{i,j} = x_{i,j+1/2} - x_{i,j-1/2}$ denotes the length of the control volume $C_{i,j}$.

The extended Euler equations are composed of the conservative Euler equations and the quasi conservative species equation. Firstly, we consider the spatial discretization for the conservative terms.

2.1. Spatial discretization for Euler equations

Following the idea of the spectral volume method for conservation laws, we integrate Eq.(1) over $C_{i,j}$ and obtain the following semi-discretized spectral volume scheme for the Euler equations

$$\frac{d\overline{W}_{i,j}}{dt} + \frac{1}{h_{i,j}}\left(\widehat{F}_{i,j+\frac{1}{2}} - \widehat{F}_{i,j-\frac{1}{2}}\right) = 0. \tag{4}$$

where $\overline{W}_{i,j}$ is the cell-average approximation of the solution vector $W = (\rho, \rho U, \rho E)^T$ over the control volume $C_{i,j}$

$$\overline{W}_{i,j} = \frac{1}{h_{i,j}} \int_{C_{i,j}} W(x,t)dx,$$

and $\widehat{F}_{i,j+\frac{1}{2}}$ denotes the numerical flux. Correspondingly, points $x_{i,j+1/2}, j = 0, 1, \ldots, \mathbf{k}$ can be viewed as the flux point.

2.1.1. Initial reconstruction

Firstly, from the cell average of $C_{i,j}$ at t^n, we can reconstruct a piecewise polynomial of degree at most $k-1$ for the spectral volume

$$W_h^n(x) = \sum_{\ell=0}^{\mathbf{k}-1} \overline{W}_i^{n,(\ell)} \phi^{(\ell)}(x - x_i) =: W_i^n(x), \quad x \in S_i, \tag{5}$$

where $\phi^{(\ell)}(x - x_i)$ is an order $k-1$ polynomial. $W_i^n(x)$ can be uniquely defined by the following relations:

$$\sum_{\ell=0}^{\mathbf{k}-1} \overline{W}_i^{n,(\ell)} \int_{C_{i,j}} \phi^{(\ell)}(x - x_i)\, dx = \int_{C_{i,j}} W_i^n(x)\, dx = h_{i,j} \overline{W}_{i,j}^n, j = 1, \ldots \mathbf{k}. \tag{6}$$

The reconstructed polynomial has the following properties:

Remark 2.1. *$W_h^n(x)$ is continuous inside each spectral volume and is discontinuous at the interface of the spectral volume.*

The above reconstruction (5) may generate spurious oscillations when the solutions contain large gradients or discontinuities. To avoid such difficulties, the detect and limit technique is needed. Here we adopt the TVB-minmod limiter based on the primitive variable for the control volumes, and the details refer to [21]. If the detector is triggered, the interface of the control volume is discontinuous and we call it "discontinuous flux points". Otherwise, it is continuous, named as "continuous flux points".

2.1.2. The NOK flux

The numerical flux $\widehat{F}_{i,j+\frac{1}{2}}$ can be constructed by GKS which is derived from Boltzmann-type equations, such as the BGK model. Here we use the

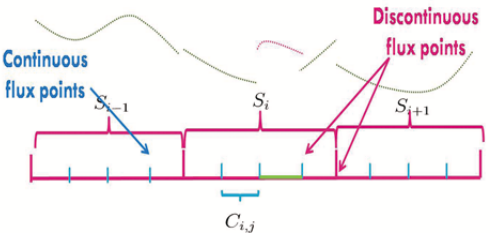

Figure 1: The initial reconstruction in each spectral volume.

non-oscillatory kinetic(NOK) flux[18] which can deal with general EOS. It is composed of two parts

$$\widehat{F}_{i,j+\frac{1}{2}} = \eta F^K_{i,j+\frac{1}{2}} + (1-\eta) F^E_{i,j+\frac{1}{2}}. \tag{7}$$

The non-equilibrium part is

$$F^K_{i,j+\frac{1}{2}} = F^+_{i,j+\frac{1}{2}} + F^-_{i,j+\frac{1}{2}},$$

where

$$F^{\pm}_{i,j+\frac{1}{2}} = \langle u^1 \rangle^{\pm}_{i,j+\frac{1}{2}} \left[\begin{array}{c} \rho \\ \rho U \\ \rho E \end{array} \right]^{L/R}_{i,j+\frac{1}{2}} + \left[\begin{array}{c} 0 \\ P^{L/R}_{i,j+\frac{1}{2}} \langle u^0 \rangle^{\pm}_{i,j+\frac{1}{2}} \\ \frac{1}{2} P^{L/R}_{i,j+\frac{1}{2}} \langle u^1 \rangle^{\pm}_{i,j+\frac{1}{2}} + \frac{1}{2} P^{L/R}_{i,j+\frac{1}{2}} U^{L/R}_{i,j+\frac{1}{2}} \langle u^0 \rangle^{\pm}_{i,j+\frac{1}{2}} \end{array} \right],$$

and

$$\langle u^0 \rangle^{\pm}_{i,j+\frac{1}{2}} = \frac{1}{2} \mathrm{erfc}(\mp \sqrt{\lambda^{\pm,*}_{i,j+\frac{1}{2}}} U^{L/R}_{i,j+\frac{1}{2}}), \quad \langle u^1 \rangle^{\pm}_{i,j+\frac{1}{2}} = U^{L/R}_{i,j+\frac{1}{2}} \langle u^0 \rangle^{\pm}_{i,j+\frac{1}{2}} \pm \frac{1}{2} \frac{e^{-\lambda^{\pm,*}_{i,j+\frac{1}{2}} (U^{L/R}_{i,j+\frac{1}{2}})^2}}{\sqrt{\pi} \lambda^{\pm,*}_{i,j+\frac{1}{2}}}.$$

And the equilibrium part is

$$F^E_{i,j+\frac{1}{2}} = \left(\begin{array}{c} \bar{\rho}\bar{U} \\ \bar{\rho}\bar{U}^2 + \bar{P} \\ \bar{\rho}\bar{E}\bar{U} + \bar{P}\bar{U} \end{array} \right)_{i,j+\frac{1}{2}},$$

where the primitive variables are calculated by

$$\left(\begin{array}{c} \bar{\rho} \\ \bar{U} \\ \bar{P} \end{array} \right)_{i,j+\frac{1}{2}} = \left(\begin{array}{c} \rho^L_{i,j+\frac{1}{2}} \langle u^0 \rangle^+_{i,j+\frac{1}{2}} + \rho^R_{i,j+\frac{1}{2}} \langle u^0 \rangle^-_{i,j+\frac{1}{2}} \\ \langle u^1 \rangle^+_{i,j+\frac{1}{2}} + \langle u^1 \rangle^-_{i,j+\frac{1}{2}} \\ P^L_{i,j+\frac{1}{2}} \langle u^0 \rangle^+_{i,j+\frac{1}{2}} + P^R_{i,j+\frac{1}{2}} \langle u^0 \rangle^-_{i,j+\frac{1}{2}} \end{array} \right),$$

and $\bar{E}$ is determined by EOS. $\lambda^{+,*}_{i,j+\frac{1}{2}}$ and $\lambda^{-,*}_{i,j+\frac{1}{2}}$ are given by

$$\lambda^{+,*}_{i,j+\frac{1}{2}} \quad = \quad \lambda^{-,*}_{i,j+\frac{1}{2}} =: \lambda_{i,j+\frac{1}{2}} = \min\Big\{\frac{1}{(c^{+}_{i,j+\frac{1}{2}})^2}, \frac{1}{(c^{-}_{i,j+\frac{1}{2}})^2}\Big\},$$

where c denotes the speed of sound. In fact, the condition that $\lambda^{+,*}_{i,j+\frac{1}{2}}$ and $\lambda^{-,*}_{i,j+\frac{1}{2}}$ are set to be equal is essential in the NOK scheme, which guarantees no oscillation will be produced near the contact discontinuities observed in original BGK and KFVS scheme even for single-material. Similar to the analysis in [18], we can prove the above scheme is consistent with the Euler equations(1). At the continuous flux points, as the state is continuous, the NOK flux reduces to

$$\widehat{F}_{i,j+\frac{1}{2}} = \left[\begin{array}{c} \rho U \\ \rho U^2 + P \\ (\rho E + P)U \end{array}\right]_{i,j+\frac{1}{2}}. \tag{8}$$

We denote it as $\widehat{F}^{C}_{i,j+\frac{1}{2}}$, the continuous NOK flux. By contrast, (7) is denoted as the discontinuous NOK flux, $\widehat{F}^{D}_{i,j+\frac{1}{2}}$. Based on the property of the initial reconstruction, at the discontinuous flux points, $\widehat{F}^{D}_{i,j+\frac{1}{2}}$ is used for numerical flux, and at the continuous flux points, the continuous NOK flux is used, which can greatly save the computational cost.

2.2. Spatial discretization for species equation

There are two different formulations of the species equation. The first one is conservative,

$$(\rho\phi)_t + (\rho u\phi)_x = 0.$$

Then the conservative spectral volume NOK scheme can be used for species equation, and the numerical scheme is

$$\frac{d\overline{\rho\phi}_{i,j}}{dt} + \frac{\eta}{h_{i,j}}(\Delta_{i,j}\rho^L\phi^L\langle u^1\rangle^+ + \Delta_{i,j}\rho^R\phi^R\langle u^1\rangle^-) + \frac{1-\eta}{h_{i,j}}\Delta_{i,j}\overline{\rho}\overline{\phi}\overline{U} = 0. \tag{9}$$

where

$$\overline{\phi}_{i,j+\frac{1}{2}} = \phi^L_{i,j+\frac{1}{2}}\langle u^0\rangle^+_{i,j+\frac{1}{2}} + \phi^R_{i,j+\frac{1}{2}}\langle u^0\rangle^-_{i,j+\frac{1}{2}}.$$

Here we introduce

$$\Delta_{i,j}\rho = \rho_{i,j+\frac{1}{2}} - \rho_{i,j+\frac{1}{2}}$$

for notation. However, oscillations of velocity and pressure will be produced, see Example 2 in Section 3. The reason of oscillations can be analyzed following the principle introduced by Abgrall[2]. The main idea is that for compressible flows with material interfaces, the necessary condition should be satisfied, i.e., if the velocity and pressure are constant at the initial time $U^n = U_0, P^n = P_0$, they should keep constant at the next time level: $U^{n+1} = U_0, P^{n+1} = P_0$.

From the current spatial reconstruction, we can get that:

$$U^L_{i,j+\frac{1}{2}} = U^R_{i,j+\frac{1}{2}} = U_0, \quad P^L_{i,j+\frac{1}{2}} = P^R_{i,j+\frac{1}{2}} = P_0. \tag{10}$$

And in the NOK flux, it holds that:

$$< u^0 >^+ + < u^0 >^- = 1, \quad < u^1 >^+ + < u^1 >^- = U_0. \tag{11}$$

The semi-discretized scheme for the continuity equation can be written in the following form:

$$\frac{d\overline{\rho}_{i,j}}{dt} + \frac{\eta}{h_{i,j}}(\Delta_{i,j}\rho^L < u^1 >^+ + \Delta_{i,j}\rho^R < u^1 >^-) + \frac{1-\eta}{h_{i,j}}U_0(\Delta_{i,j}\rho^L < u^0 >^+ + \Delta_{i,j}\rho^R < u^0 >^-) = 0. \tag{12}$$

Similarly, the discretization for the momentum equation can be written as

$$\frac{d\overline{\rho U}_{i,j}}{dt} + \frac{\eta}{h_{i,j}}(\Delta_{i,j}\rho^L U^L < u^1 >^+ + \Delta_{i,j}\rho^R U^R < u^1 >^-) + \frac{1-\eta}{h_{i,j}}U_0^2(< \Delta_{i,j}\rho^L < u^0 >^+ + \Delta_{i,j}\rho^R < u^0 >^-) = 0. \tag{13}$$

Combined with (12), and based on the two properties (10)(11), we can derive from (13) that the velocity can keep constant, i.e., $\frac{d\overline{U}_{i,j}}{dt} = 0$. The discretization for energy is

$$\frac{d\overline{\rho E}_{i,j}}{dt} + \frac{\eta}{h_{i,j}}(\Delta_{i,j}\rho^L E^L < u^1 >^+ + \Delta_{i,j}\rho^R E^R < u^1 >^-) + \frac{1-\eta}{h_{i,j}}U_0\Delta_{i,j}\overline{\rho}\overline{E} = 0. \tag{14}$$

From (14), substituting the EOS, we get that it is enough to guarantee constant pressure $P^{n+1} = P_0$ if the following condition is satisfied,

$$\begin{aligned}
&\frac{d}{dt}(\frac{1}{\gamma-1})_{i,j} + \frac{\eta}{h_{i,j}}(\Delta_{i,j}(\frac{1}{\gamma-1})^L < u^1 >^+ + \Delta_{i,j}(\frac{1}{\gamma-1})^R < u^1 >^-) \\
&\qquad + \frac{1-\eta}{h_{i,j}} U_0(\Delta_{i,j}\frac{1}{\gamma-1}) = 0, \\
&\frac{d}{dt}(\frac{\gamma P_\infty}{\gamma-1})_{i,j} + \frac{\eta}{h_{i,j}}(\Delta_{i,j}(\frac{\gamma P_\infty}{\gamma-1})^L < u^1 >^+ + \Delta_{i,j}(\frac{\gamma P_\infty}{\gamma-1})^R < u^1 >^-) \\
&\qquad + \frac{1-\eta}{h_{i,j}} U_0(\Delta_{i,j}\frac{\gamma P_\infty}{\gamma-1}) = 0. \qquad (15)
\end{aligned}$$

And following the idea of Shyue[4], if every component of specie variable is discretized by

$$\begin{aligned}
&\frac{dY_{i,j}}{dt} + \frac{\eta}{h_{i,j}}(\Delta_{i,j}Y^L < u^1 >^+ + \Delta_{i,j}Y^R < u^1 >^-) + \frac{1-\eta}{h_{i,j}}(\Delta_{i,j}Y^L U^L < u^0 >^+ \\
&\qquad + \Delta_{i,j}Y^R U^R < u^0 >^-) - Y_{i,j}(\Delta_{i,j} < u^1 >^+ + \Delta_{i,j} < u^1 >^-) = 0, \qquad (16)
\end{aligned}$$

the condition (15) will be satisfied, which can guarantee non-oscillatory velocity and pressure near the material interfaces. And at the meantime, (16) can be viewed as the discretization of the quasi-conservative form of the species equation

$$Y_t + (UY)_x = YU_x. \qquad (17)$$

For time integration, we employ the nonlinearly Runge-Kutta time discretization. The above semi-discrete scheme can be written as

$$\frac{d\overline{W}_{i,j}}{dt} = L(\overline{W}).$$

In our computations, the classical fourth order Runge-Kutta method[24] is used,

$$\begin{aligned}
\overline{W}^{(1)}_{i,j} &= \overline{W}^n_{i,j} + \frac{1}{2}\Delta t L(\overline{W}^n), \\
\overline{W}^{(2)}_{i,j} &= \overline{W}^n_{i,j} + \frac{1}{2}\Delta t L(\overline{W}^{(1)}), \\
\overline{W}^{(3)}_{i,j} &= \overline{W}^n_{i,j} + \Delta t L(\overline{W}^{(2)}), \\
\overline{W}^{n+1}_{i,j} &= \frac{1}{3}(\overline{W}^{(1)}_{i,j} + 2\overline{W}^{(2)} + \overline{W}^{(3)}_{i,j} - \overline{W}^n_{i,j}) + \frac{1}{6}\Delta t L(\overline{W}^{(3)}). \qquad (18)
\end{aligned}$$

with the time step size Δt_n determined by

$$\Delta t_n = \frac{\alpha \min h_{i,j}}{\max\{|\overline{U}_{i,j}| + \bar{c}_{i,j}\}}, \tag{19}$$

where the constant α denotes the CFL number.

3. Numerical tests

In this section, we run the present scheme for various order on several examples, and we should point out that actually the present scheme can be implemented to arbitrary high order in space dimension. In all the numerical computations, we divide the computational domain into several uniform spectral volumes, which is simple but not necessary. And the Gauss-Lobatto points[21] are used to partition the spectral volume. α in (19) is set to be 0.8 for one-dimensional case and 0.5 for two-dimensional case, and the artificial coefficient M in the TVB-minmod limiter is set to be 50 if not specified.

Example 1. Accuracy test. To begin with, we consider a sine wave composed of two components with the initial condition

$$\rho(x,0) = 1 + 0.2\sin(\pi x), \quad U(x,0) = 0.7,$$
$$P(x,0) = 1, \quad \gamma(x,0) = \begin{cases} 1.4, & 0 \le x \le 1, \\ 1.9, & 1 \le x \le 2. \end{cases}$$

The computational region is defined on $[0,2]$ and the periodic boundary condition is used. The exact solution for this problem is

$$\rho(x,t) = 1 + 0.2\sin(\pi(x - 0.7t)), \quad U(x,t) = 0.7, \quad P(x,t) = 1.$$

with $\gamma = 1.4$ when $y > 0$ and $\gamma = 1.9$ when $y < 0$.

The numerical results are shown in Table 1. We can see that the present scheme up to fifth order can achieve their designed order accuracy.

Example 2 . The interface only problem. The initial condition are listed below:

$$(\rho, u, P, \gamma, P_\infty) = \begin{cases} (1,1,1,1.4,1), & x \le 0.5, \\ (0.125,1,1,1.9,0), & else. \end{cases}$$

Table 1: Errors and numerical orders of accuracy of the present scheme for Example 1.

	$k=2$		$k=3$		$k=4$		$k=5$	
N	L^2_{err}	L^2_{ord}	L^2_{err}	L^2_{ord}	L^2_{err}	L^2_{ord}	L^2_{err}	L^2_{ord}
10	5.27E-3	-	3.68E-4	-	8.70E-6	-	4.90E-7	-
20	1.32E-3	2.00	5.45E-5	2.76	5.40E-7	4.01	1.73E-8	4.82
40	3.32E-4	1.99	7.25E-6	2.91	3.21E-8	4.07	5.82E-10	4.89
80	8.33E-5	1.99	9.26E-7	2.97	2.01E-9	4.00	1.86E-11	4.97
160	2.09E-5	1.99	1.17E-7	2.98	1.25E-10	4.01	5.34E-13	5.12

The computation is performed on 100 cells and we compute the solution up to 0.1. According to our analysis, numerical oscillations of velocity and pressure are expected for the fully conservative scheme. This is confirmed by numerical simulation, see Fig.2, where remarkable oscillations of velocity and pressure are observed near the material interfaces and soon spread into density. Then we implement this test by the present quasi-conservative SVNOK scheme. Fig.3 shows the profiles of density, heat ratio, pressure, velocity for the implementations of the current scheme of various order of accuracy. Obviously, there is no spurious oscillation across the material interface in the velocity and pressure, and higher order scheme resolves better than lower order scheme. To compare our SVNOK scheme with the original second order NOK scheme[18], we give the close-up of the density near the material interface in Fig.4, from which we can observe that the second-order SVNOK scheme can compete with the original second-order NOK scheme. That is because the compact reconstruction procedure supplies more information than MUSCL scheme which is used in the original second order NOK scheme. And the higher order scheme shows better resolution. (Note: The exact solution in the right figure of Fig.4, which is the right figure of Fig.4 in [18], is obtained by exact solution on 100 uniform grid points. Actually the interface should be exactly located at 0.6.)

Example 3. The square wave problem. In this test, the square wave is propagated at a constant speed of one subject to periodic boundary conditions.

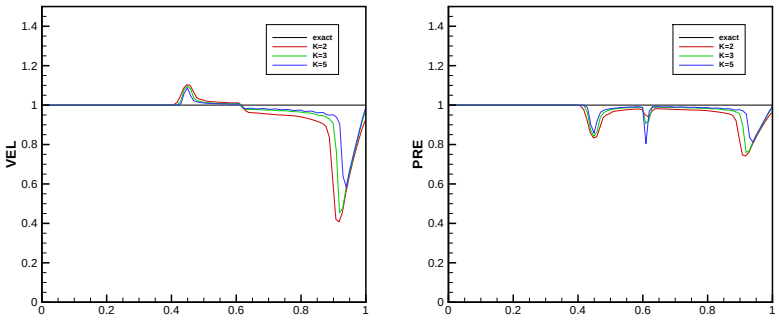

Figure 2: Example 2: velocity(left) and pressure(right) profiles for conservative spectral volume scheme. The black solid line: Exact solution.

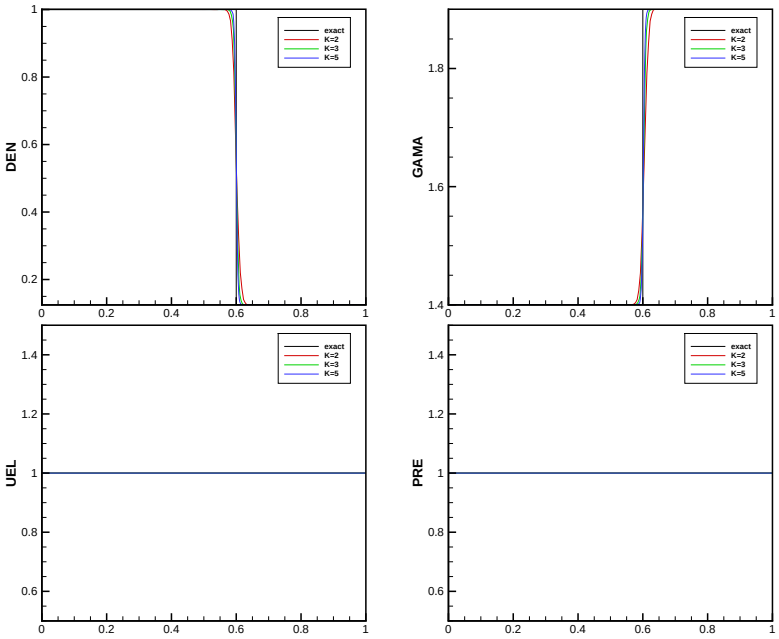

Figure 3: Example 2: The density(top left), γ(top right), velocity(bottom left) and pressure(bottom right) profiles for the present quasi-conservative SVNOK schemes. The black solid line: Exact solution.

The initial condition are given by:

$$(\rho, u, P, \gamma, P_\infty) = \begin{cases} (1.1, 1, 1, 1.6, 0), & 0.25 \leq x \leq 0.75, \\ (0.1, 1, 1, 1.4, 1), & else. \end{cases}$$

We carry out the computation with forty spectral volumes. In Fig.5 the

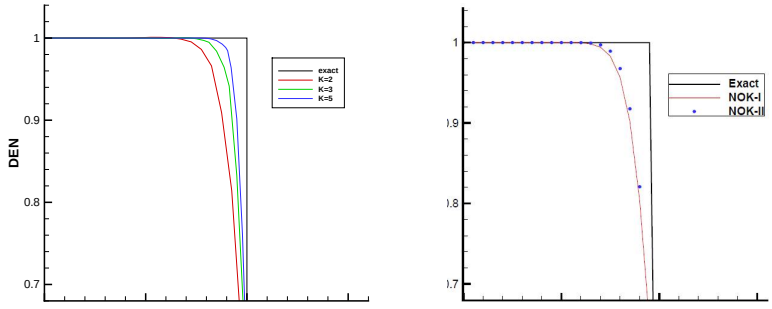

Figure 4: Example 2: Close-up of the density near the material interface. Left: Results of the SVNOK schemes. Right: Results of second order NOK scheme[18].

numerical results at time $t = 1.0$ are shown. Note first that the pressure and velocity are indeed nonoscillatory near the material interface, and the material interface is captured with higher resolution by using higher order schemes. This test is quite similar to the one in [21] which is simulated by the linear advection equation calculated by the spectral volume method. Fig.6 shows the density profiles for the second-, fifth-, seventh-, twelfth-order schemes, respectively. Compared with the results in [21], we observe that the present scheme has similar resolution with the original spectral volume method. Then to study the long-term performance of the present method, we simulate this test for 50 periods. In this test, TVD limiter is used to avoid numerical oscillations during the long term simulation. Fig.7 shows the profiles of density, heat ratio, velocity, and pressure for the second-, fifth-, seventh-, and twelfth-order schemes after the square wave crosses the computational domain 50 times. It is obvious that the result for low order scheme smears after long term simulation, and the fifth-order scheme also dissipates the square wave much more than the seventh- and twelfth-order schemes. But all order of schemes preserve nonoscillatory near the material interface, which demonstrates the good performance of our scheme when simulating multi-component flows. Fig.8 shows the density profiles for the seventh-, twelfth-order schemes, respectively, which are in good agreement with those in [21], while they all preserve the square wave quite well after 50 periods.

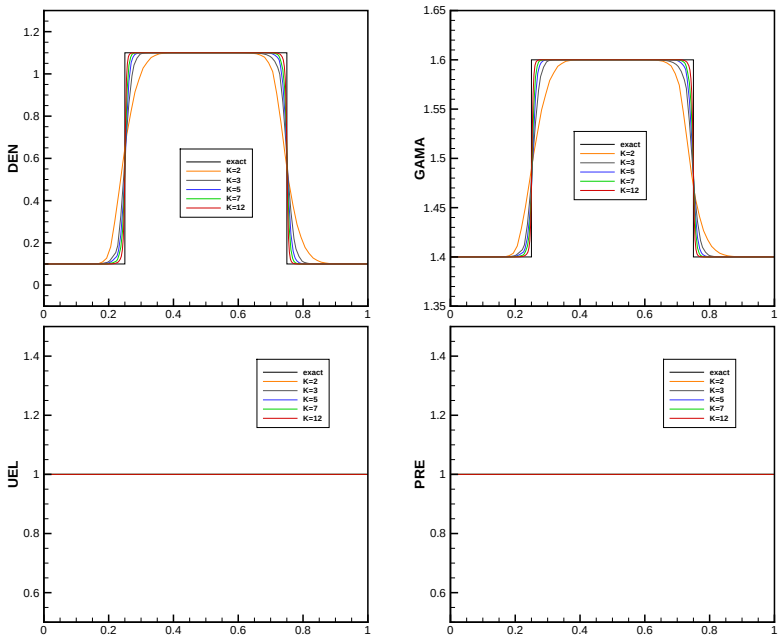

Figure 5: Example 3: The density(top left), γ(top right), velocity(bottom left) and pressure(bottom right) profiles by the SVNOK schemes at $t = 1$. The black solid line: Exact solution.

Example 4. Shock and sine wave interaction. The example is first introduced by Shu and Osher in [25] for single material, which describes the interaction of a right moving shock wave with a sine wave in density. It has been widely used to test the numerical (artificial) viscosity of the scheme. Here we verify it to two different components. The initial condition is taken as:

$$(\rho, u, P, \gamma, P_\infty) = \begin{cases} (3.857134, 2.629369, 10.33333, 1.4, 1), & -5 \le x \le -4, \\ (1 + 0.2sin(5x), 0, 1, 1.6, 0), & -4 \le x \le 5. \end{cases}$$

The computation is performed until $t = 1.8$ by using the SVNOK scheme from second to fifth order. Fig.9 plots the density in the computational domain $[-5, 5]$ and the interval $[0, 3]$ on various scales of grids. The reference solution is obtained by using the second order scheme with a fine mesh of 10000 cells. The shock wave interacts with the sine wave and generates some complex but smooth structures at the left hand side of the shock wave, which is very similar to the single material case but with clear material interface as dividing line. With

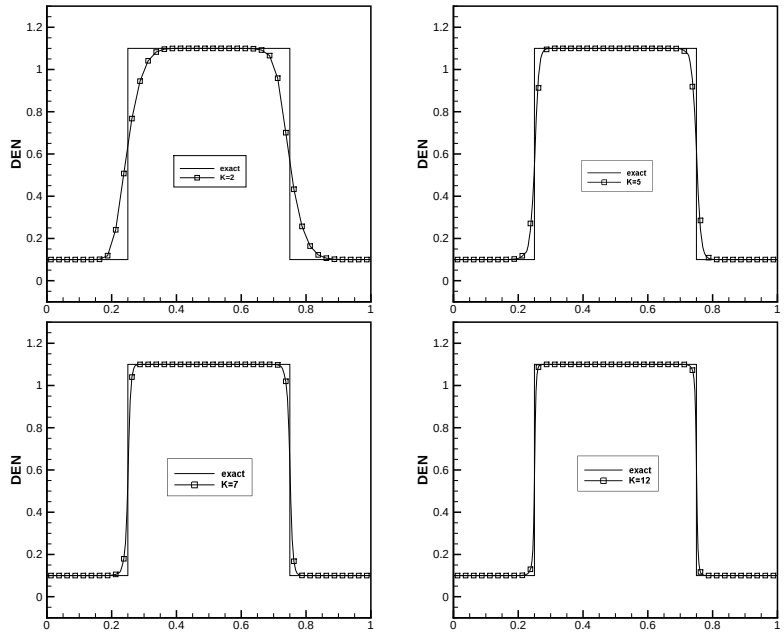

Figure 6: Example 3: The density profiles for the second-(top left), fifth-(top right), seventh-(bottom left), twelfth-(bottom right)order at $t = 1$.

400 spectral volumes, schemes up to fifth order have not converged, but higher order scheme is obviously better for resolving those complex structures. With 600 spectral volumes, fifth-order scheme almost converges to the exact solution except for the interval of material interface. With 1000 spectral volumes, fifth-order scheme converges to the exact solution even near material interface, while second- and third-order schemes have not converged near material interface. This demonstrates that higher order scheme is obviously better in resolving those complex structures as well as the discontinuities.

Example 5. Gas-liquid shock tube test with a strong shock wave. We consider a Riemann problem using the following initial condition:

$$(\rho, u, P, \gamma, P_\infty) = \begin{cases} (10^3, 0, 10^9, 4.4, 6 \times 10^8), & -0.2 \le x \le 0.5, \\ (50, 0, 10^5, 1.4, 0), & 0.5 \le x \le 1. \end{cases}$$

This is a very challenging test case with a strong shock wave while the shock and the material interface are very close. We carry out the computation with

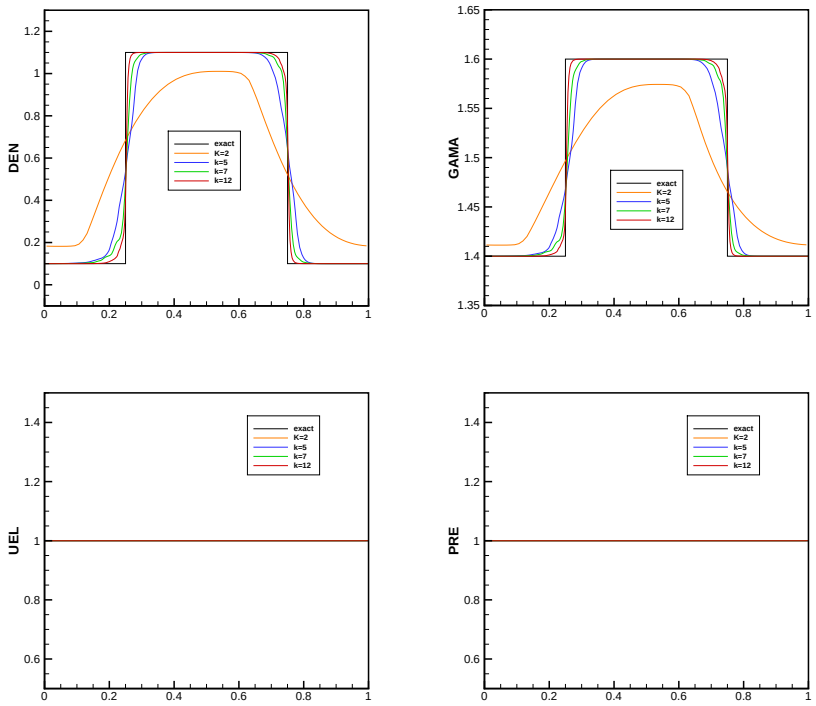

Figure 7: Example 3: The density(top left), γ(top right), velocity(bottom left) and pressure(bottom right) profiles by the present schemes at $t = 50$. The black solid line: Exact solution.

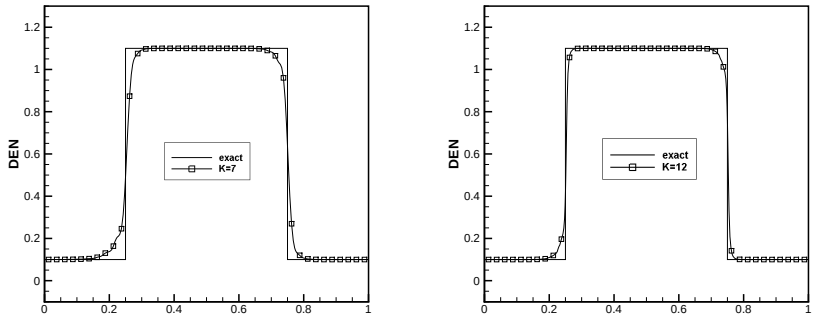

Figure 8: Example 3: The density profiles for the seventh-(left) and twelfth-(right)order at $t = 50$.

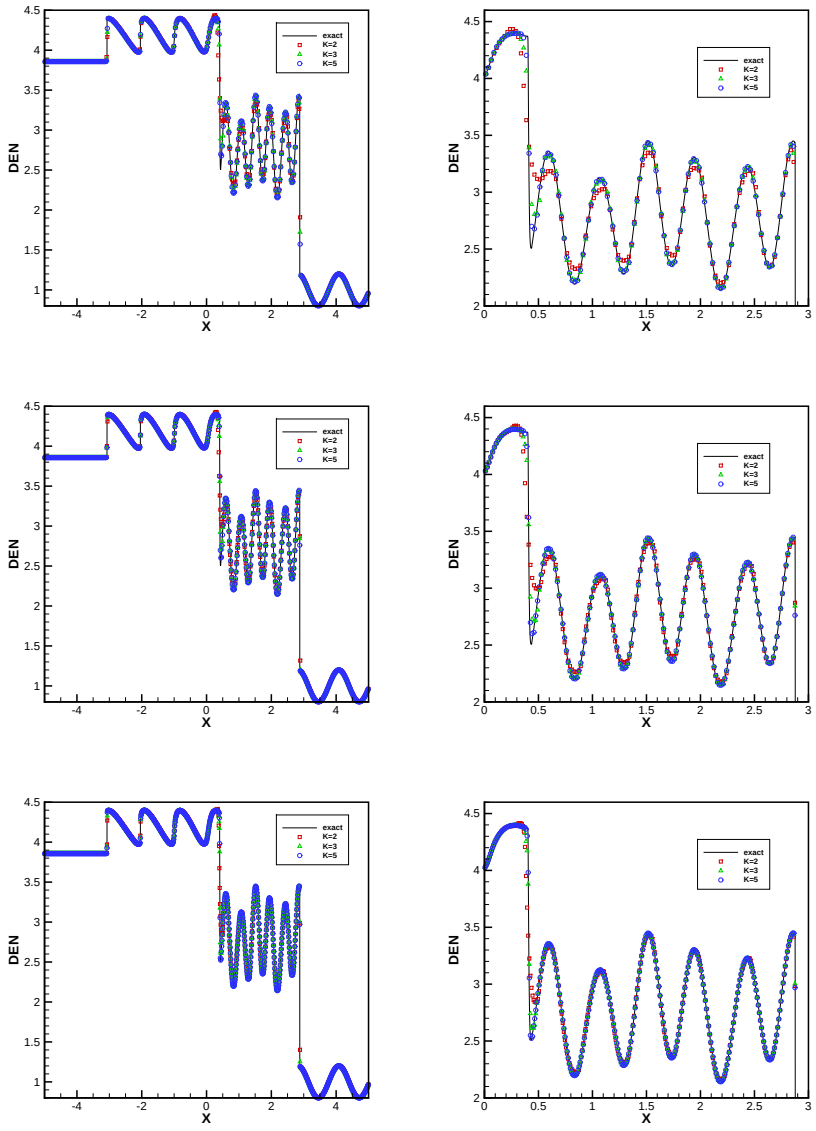

Figure 9: Example 4: The density(left) and the close-up(right) profile at time $t = 1.8$ by the SVNOK schemes various orders of accuracy. Top: N=400; Middle: N=600, Bottom: N=1000.

1000 cells at terminal time $t = 0.0002$. Fig.10 shows the profiles of density, heat ratio, pressure, velocity for the implementations of the SVNOK scheme from

second to fifth order. Fig.11 shows the close-up density profiles near the rarefaction and material interface, respectively, from which we can reach the same conclusion as for other cases that higher order scheme shows better resolution. To compare with the result of the original second order NOK scheme[18] with 10000 cells, we implement our SVNOK scheme with 2000 cells. As shown in Fig.12, it is clear to see that although second-order SVNOK scheme only use 2000 cells, its resolution can compete the original second order NOK scheme with 10000 cells even with less transition points near the material interface, and fifth order scheme wins higher resolution. This demonstrates the good performance of our scheme in resolving discontinuities.

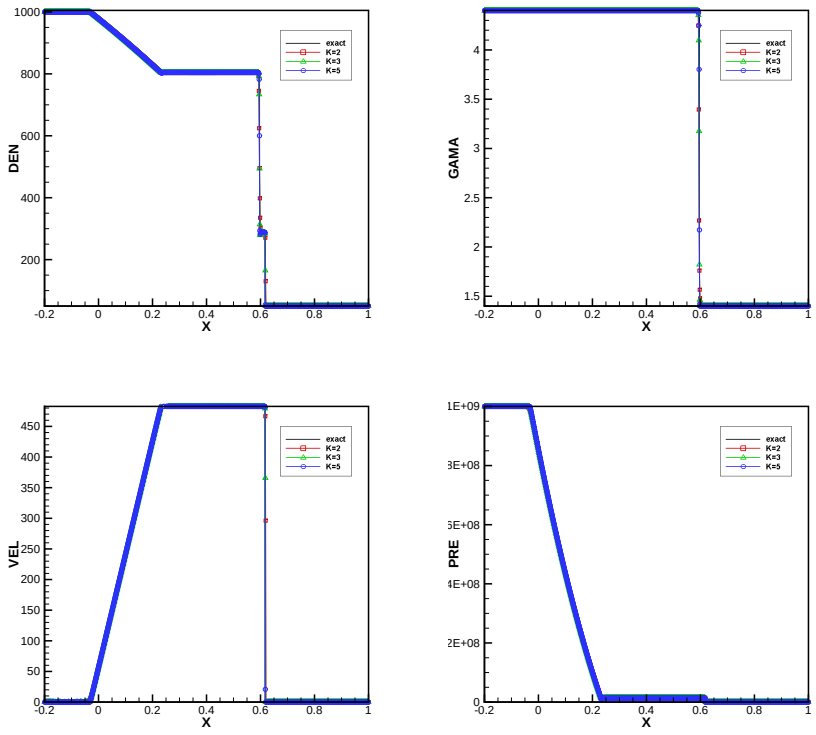

Figure 10: Example 5: The density(top left), γ(top right), velocity(bottom left) and pressure(bottom right) profiles for the SVNOK schemes with 1000 cells at time $t = 0.0002$. The black solid line: Exact solution.

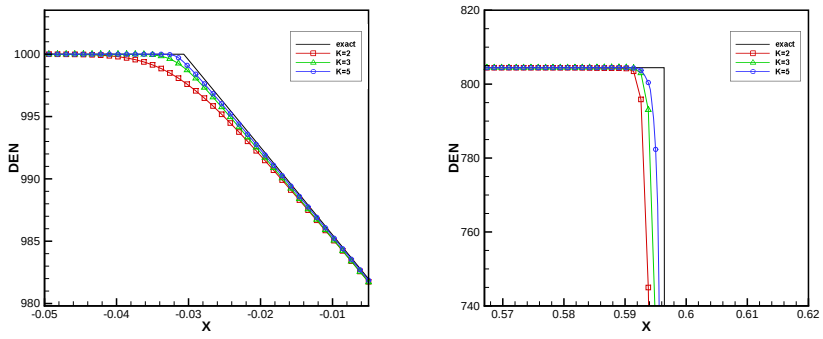

Figure 11: Example 5: Close-up of the density near the rarefaction(left) and material interface(right).

Example 6. Two dimensional Richtmyer-Meshkov instability problem. In the computational domain $[-2, 2] \times [-0.5, 0.5]$, there are two kinds of fluids. The heavy one is SF_6 and the light one is the air. They are separated by a perturbed interface, which initial shape is generated by

$$f(y) = 1.2 + 0.1 \cos(2\pi y).$$

The initial conditions are

$$(\rho, U, V, P, \gamma, P_\infty) = \begin{cases} (1, 0, 0, 1, 1.4, 0), & x \le f(y), \\ (5, 0, 0, 1, 4, 1), & x \le 1.325, \\ (7.093, -0.7288, 0, 10, 4, 1), & else. \end{cases}$$

The top and bottom boundary are periodic, while the left and right boundary are non-reflecting. At the beginning, the shock wave propagates from SF_6 to the air. Then the perturbed interface is shifted when the shock wave captures it, and forms very complex wave structure. We carry out the computation with 320×80 cells and simulate up to $t = 2$. The density contours with 30 equally spaced contour lines obtained by the second-, third-, fifth-order SVNOK scheme are shown in Fig.13, comparing with the reference result by second order NOK scheme[18]. Clearly, the result obtained by the second-order SVNOK scheme has better resolution than the second order NOK scheme[18], and the higher order

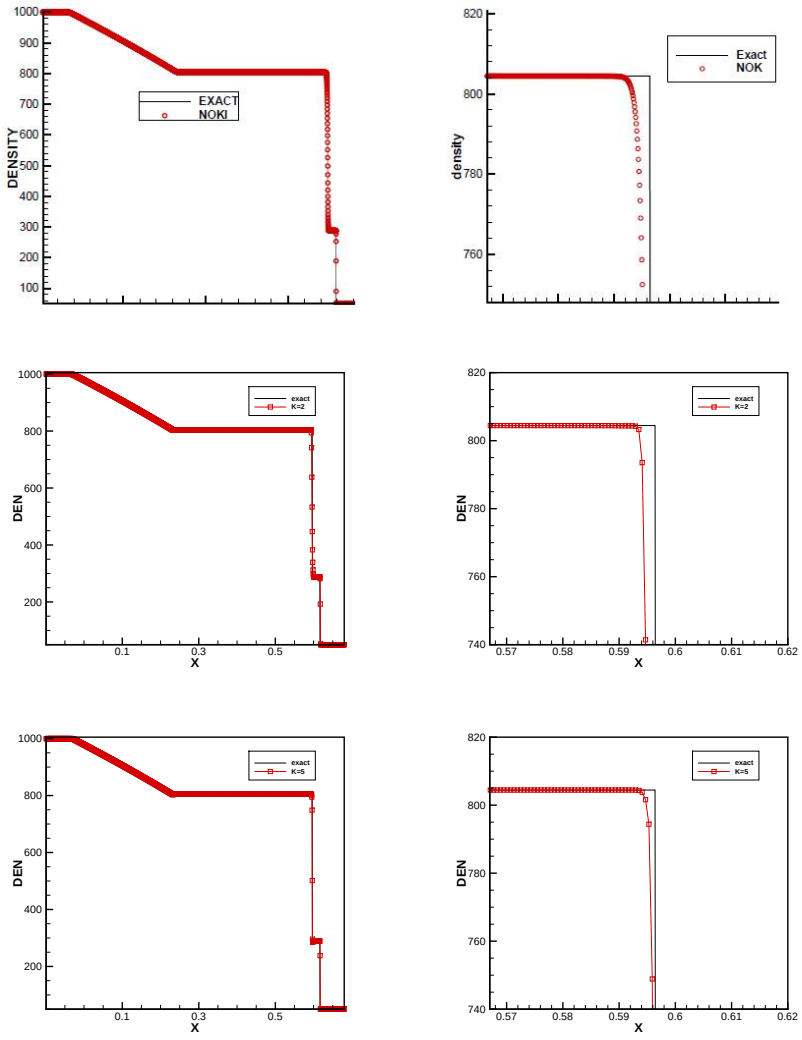

Figure 12: Example 5: The density(left)and its close-up(right) profiles at time $t = 0.0002$. Top: second order NOK scheme[18] with 10000 cells; Middel: the present second-order scheme with 2000 cells. Bottom: the present fifth-order scheme with 2000 cells.

scheme can better capture the complicate pattens appeared in the interaction process between the shock wave and the perturbed interface.

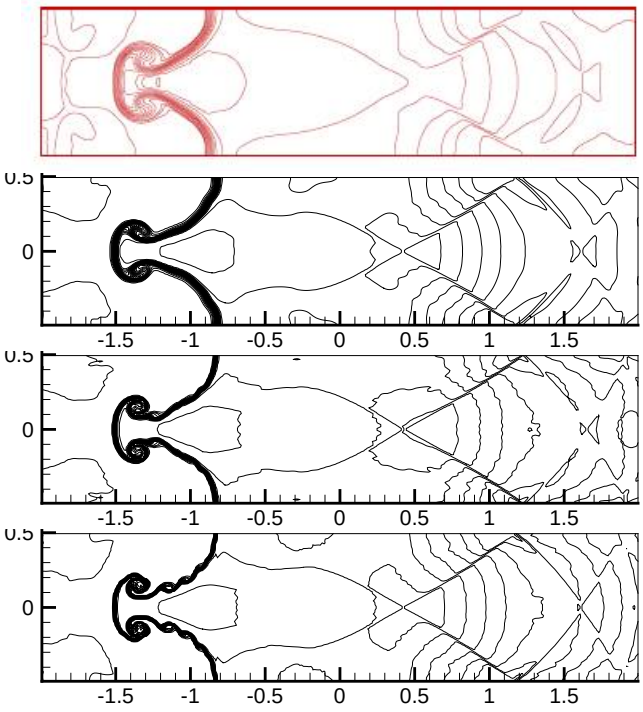

Figure 13: Example 6: The density contours at time $t = 2$ with 30 equally spaced contour lines ranging from 2.2 to 6. The figure from top to bottom are the reference result by second order NOK scheme[18], the result by the second-, third-, fifth-order SVNOK scheme, respectively.

4. Conclusion

185

In this paper, a high-order, stencil-compact gas kinetic scheme named spectral volume non-oscillatory kinetic(SVNOK) scheme is proposed for multi-component flows with a stiffened gas equation of state. Here, we focus on the quasi-conservative extended Euler equations, which is one of popular models of multi-
190 component flows. This model can be separated into two parts: the conservative part and the non-conservative part. The original high order compact SV scheme is used to discretize the conservative part directly. The main modification is that the NOK scheme is used to compute the numerical flux to deal with the stiffened

gas EOS. Then, the numerical scheme for the non-conservative part is carefully considered. To avoid unphysical oscillation near the material interfaces, a necessary condition is introduced to analyze the numerical scheme. Starting from this condition, after some non-trivial numerical deductions, a high order compact SV scheme with NOK flux for the non-conservative part is obtained. Thus the new scheme not only can achieve high order accuracy with compact stencil, but also can avoid the unphysical pressure and velocity oscillations near the material interfaces. We have carried out a number of 1D and 2D numerical tests to demonstrate the good performance of the new scheme. Numerical results show the new scheme can achieve the desired high order accuracy without introducing unphysical oscillation near the material interfaces. In addition, comparing to the original NOK scheme[18], the new scheme improves the resolution significantly.

References

[1] S. Karni, Multicomponent flow calculations by a consistent primitive algorithm, J. Comput. Phys. 112 (1) (1994) 31–43.

[2] R. Abgrall, How to prevent pressure oscillations in multicomponent flow calculation: A quasi conservative approach, J. Comput. Phys. 125 (1) (1996) 150–160.

[3] S. Karni, Hybrid multi-fluid algorithm, SIAM J. Sci. Comput. 17 (1996) 1019–1039.

[4] K. M. Shyue, An effcient shock-capturing algorithm for compressible multicomponent problems, J. Comput. Phys. 142 (1) (1998) 208–242.

[5] K. M. Shyue, A fluid-mixture type algorithm for compressible multicomponent flow with Mie-Gruneisen equation of state, J. Comput. Phys. 171 (2) (2001) 678–707.

[6] K. Xu, A kinetic method for hyperbolicelliptic equations and its application in two-phase flow, J. Comput. Phys. 166 (2) (2001) 383–399.

[7] K. Xu, K. H. Prendergast, Numerical Navier-Stokes solutions from gas kinetic theory, J. Comput. Phys. 114 (1) (1994) 9–17.

[8] K. Xu, L. Martinelli, A. Jameson, Gas-kinetic finite volume methods, flux vector splitting, and artificial diffusion, J. Comput. Phys. 120 (1) (1995) 48–65.

[9] Q. Li, K. Xu, S. Fu, A high-order gas-kinetic Navier-Stokes solver, J. Comput. Phys. 229 (19) (2010) 6715–6731.

[10] N. Liu, H. Z. Tang, A high-order accurate gas-kinetic scheme for one- and two-dimensional flow simulation, Commun. Comput. Phys. 15 (4) (2014) 911–943.

[11] T. Ohwada, On the construction of kinetic scheme, J. Comput. Phys. 177 (1) (2002) 156–175.

[12] K. Xu, BGK-based scheme for multicomponent flow calculations, J. Comput. Phys. 134 (1) (1997) 122–133.

[13] S. Jiang, G. X. Ni, A second-order γ model BGK scheme for multimaterial compressible flows, App. Num. Math. 57 (2) (2007) 597–608.

[14] S. Jiang, G. X. Ni, A γ model BGK scheme for compressible multifluids, Int. J. Numer. Meth. Fluids 46 (2) (2004) 163–182.

[15] H. Z. Tang, H. M. Wu, High resolution KFVS finite volume methods for multicomponent flow calculations, Chinese J. Comput. Phys. 117 (2) (2000) 179–186.

[16] Y. S. Lian, K. Xu, A gas-kinetic scheme for multimaterial flows and its application in chemical reactions, J. Comput. Phys. 163 (2) (2000) 349–375.

[17] Y. B. Chen, S. Jiang, Modified kinetic flux vector splitting schemes for compressible flows, J. Comput. Phys. 228 (10) (2009) 3582–3604.

[18] Y. B. Chen, S. Jiang, A non-oscillatory kinetic scheme for multicomponent flows with the equation of state for a stiffned gas, J. Comput. Math. 29 (6) (2011) 661–683.

[19] E. Johnsen, T. Colonius, Implementation of WENO schemes in compressible multicomponent flow problems, J. Comput. Phys. 219 (2) (2006) 715–732.

[20] J. Zhu, J. X. Qiu, T. G. Liu, B. C. Khoo, RKDG methods with WENO type limiters and conservative interfacial procedure for one-dimensional compressible multi-medium flow simulations, App. Num. Math. 61 (4) (2011) 554–580.

[21] Z. J. Wang, Spectral (finite) volume method for conservation laws on unstructured grids: basic formulation, J. Comput. Phys. 178 (1) (2002) 210–251.

[22] Z. J. Wang, Y. Liu, Spectral (finite) volume method for conservation laws on unstructured grids iii: one dimensional systems and partition optimization, J. Sci. Comput. 20 (1) (2004) 137–157.

[23] Z. J. Wang, L. P. Zhang, Y. Liu, Spectral (finite) volume method for conservation laws on unstructured grids iv: extension to two-dimensional systems, J. Comput. Phys. 194 (2) (2004) 716–741.

[24] G. S. Jiang, C. W. Shu, Efficient Implementation of Weighted ENO Schemes, J. Comput. Phys. 126 (1996) 202–228.

[25] C. W. Shu, S. Osher, Efficient implementation of essentially non-oscillatory shock-capturing schemes, ii, J. Comput. Phys. 83 (1) (1989) 32–78.